Controllability Analysis of an Ethanol Water Distillation Column

Willem Adriaan Smit
14052131

CBT

2019-05-23

Controllability Analysis of an Ethanol Water Distillation Column

Willem Adriaan Smit

14052131

Department of Chemical Engineering
University of Pretoria

CBT

2019-05-23

Controllability Analysis of an Ethanol Water Distillation Column

Synopsis

The controllability analysis of an ethanol water binary distillation column was conducted. The model for the column was obtained from research done by Ogunnaike et al. (1983). The method used for the controllability analysis is outlined by Skogestad & Postlethwaite (2001).

There are some limitations on the system's bandwidth due to open right hand plane poles and delays inherent to the system. It was proven that the bounds set for disturbance rejection and set-point variation were too widely spaced. The system would not be able to reject far reaching disturbances, or track far reaching set-points. An uncertainty model was also developed successfully, and together with the development of a performance weighting function the system can now be tested for robust stability and performance when the controller design takes place.

It is recommended that the bound on upper and lower disturbances to reject, or set-points to track, be re-evaluated. If the bounds are immovable it is recommended that the sizing of the final control elements be re-evaluated.

Contents

List of Figures

List of Tables

1 Introduction

Renewable energy is becoming a major role player in the world today. As people are starting to shift away from fossil fuel based technology and energy generation, the focus is shifting to alternative methods of energy (and fuel) production.

One such a method involves the use of ethanol as an alternative fuel. Ethanol particularly is an excellent contender for a major alternative fuel, as it can be produced from crops or by means of biological fermentation. [A lot of] research is currently done on methods to generate ethanol in order for it to power the future.

Producing ethanol, however, is not the only problem to overcome. After the production process (usually from fermentation (Henstra et al., 2007)), the ethanol has to be separated from the product mixture in order to purify it. This poses to be a challenge (and a very energy intensive operation) due to the thermodynamic properties of the homogeneous mixture between water and ethanol. As noted in Figure 1, the system contains an azeotrope (Wankat, 2012). This leads to very expensive separation operations, as pressure swing distillation has to be implemented for high purity separation (Green & Perry, 2007).

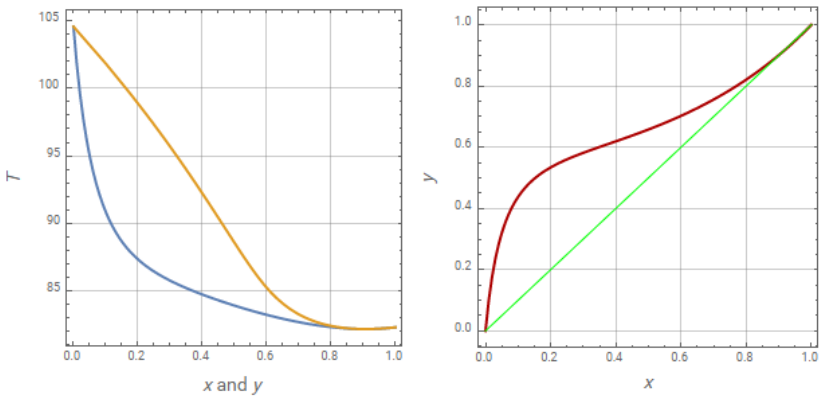

Figure 1: Vapour Liquid Equilibrium (VLE) data for the water ethanol system at 1 bar.

In this report, an investigation regarding the controllability of the ethanol water separation process is investigated. The plant investigated is a pilot plant that is testing the feasibility for scale up of the process. Control has to implemented to ensure that the system reaches a steady state, as well as to improve the overall profitability by reducing the standard deviation in the product quality.

A plant wide control system will not be investigated. Only the distillation coloumn is analysed. The current proposed control system is discussed in Section 2. This report will investigate the validity of such a proposed control scheme, as well as where the physical constrains in the system lies.

2 Process Model Description

2.1 System Diagram

The Process Flow Diagram of the system, with all the relevant inputs, outputs and disturbances are displayed in Figure 2.

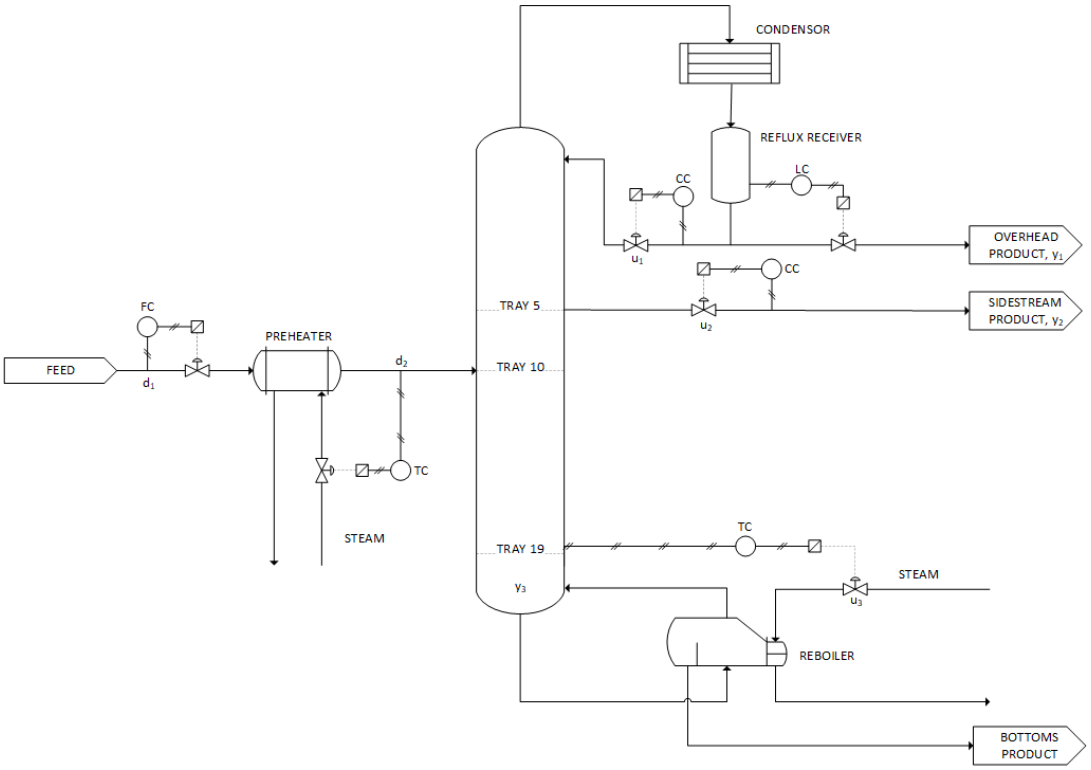

Figure 2: Process flow diagram of the system

2.2 System Description

The system involves the separation of water and ethanol (in a solution), with the aim of producing an ethanol product that can be used as an alternative fuel source.

The system can be summarized as follows:

- The distillation column of the pilot scale plant is a 19 tray, 12 inch diameter column.
- The column has variable feed and side stream draw off locations.
- The side stream flow is varied to control the composition of the stream.

- The distillate vapour draw off stream is fully condensed, and then separated into the reflux and product streams.
- The product stream is set to control the level in the condenser, while the reflux stream controls the composition of the distillate product.
- A kettle re-boiler is used to add energy to the column. Stream is the main utility.
- The amount re-boiled bottoms product is controlled by varying the steam supplied to the re-boiler.
- The feed temperature and flow rate can be controlled to simulate disturbances on the system. These variables are strictly defined as disturbances, as they are part of another section's (the bio-reactor or chemostat) control scheme.
- Currently all variables are controlled with single input single output (SISO) control loops.

2.3 Measurement of Variables

The compositions are measured/determined through various on-line sensors (densitrometry and refractometry). Temperatures are monitored using thermocouples. Flow rates are measured with thermal mass flow meters. Levels are measured by inference from static head, measured with a pressure sensor. The product model and serial numbers are not available.

2.4 System Variables

All variables in the ethanol water distillation coloumn system is summarised in Table 1. The current steady state values hold reference to the tested conditions on site.

Table 1: Summary of all the model variables.

Input Variables			
Variable	Description	Steady State Value	Units
u_1	Reflux flow rate	0.18	gpm
u_2	Side stream product flow rate	0.046	gpm
u_3	Reboiler steam pressure	20	psi
Output Variables			
Variable	Description	Steady State Value	Units
y_1	Overhead ethanol mole fraction	0.7	-
y_2	Side stream ethanol mole fraction	0.52	-
y_3	Tray #19 temperature	92	°C
Disturbance Variables			
Variable	Description	Steady State Value	Units
d_1	Feed flow rate	0.8	gpm
d_2	Feed temperature	78	°C

2.5 System Model

The model was determined by conducting step testing on the system. In most cases a first order plus dead time model gave a sufficiently accurate fit to experimental data. The sum of squares of an adequate fit during model development was a values of greater than 0.98 (Ogunnaike et al., 1983). In some relationships more complex dynamics had to be derived and a second order system with a first order lag and dead time, was used to accurately describe the impulse response (based on the same adequate fit method described above). The equations used for fitting were

$$\frac{y_i(s)}{u_i(s)} = \frac{K_i e^{-\theta_i s}}{\tau_i s + 1} \tag{1}$$

for the first order plus dead time system, and

$$\frac{y_i(s)}{u_i(s)} = \frac{K_i(\tau_{1i} s + 1)e^{-\theta_i s+1}}{(\tau_{2i} s + 1)(\tau_{3i} s + 1)} \tag{2}$$

for the relationships with more complex dynamics.

The fitting curves of two pulse tests are displayed in Figure 3 and Figure 4. An important

thing to note is that the unit of time is minutes, and therefore all responses and analysis will be conducted with this unit for time.

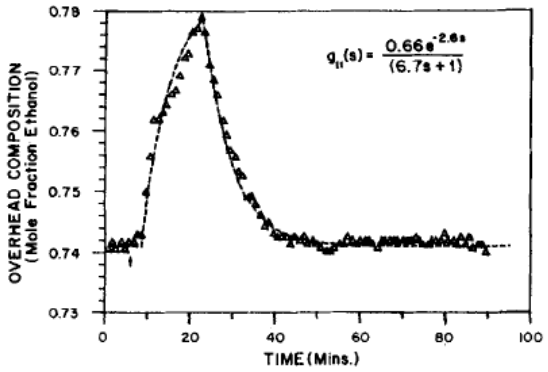

Figure 3: Overhead composition response to a pulse of 15 minutes duration in the reflux rate.

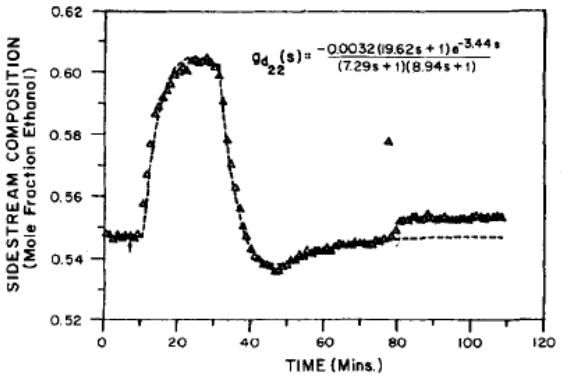

Figure 4: Side stream composition response to a pulse of 15 minutes duration in feed temperature.

The model was then written in the standard form of a linear MIMO system (Ogunnaike et al., 1983),

$$\mathbf{y}(s) = \mathbf{G}(s)\mathbf{u}(s) + \mathbf{G}_d(s)\mathbf{d}(s) \tag{3}$$

where

$$\hat{G}(s) = \begin{bmatrix} G_{11} & G_{12} & G_{13} \\ G_{21} & G_{22} & G_{23} \\ G_{31} & G_{32} & G_{33} \end{bmatrix} = \begin{bmatrix} \frac{0.66e^{-2.6s}}{6.7s+1} & \frac{-0.61e^{-3.5s}}{8.64s+1} & \frac{-0.0049e^{-s}}{9.06s+1} \\ \frac{1.11e^{-6.5s}}{3.25s+1} & \frac{-2.36e^{-3s}}{5.0s+1} & \frac{-0.012e^{-1.2s}}{7.09s+1} \\ \frac{-34.68e^{-9.2s}}{8.15s+1} & \frac{46.2e^{-9.4s}}{10.9s+1} & \frac{0.87(11.61s+1)e^{-s}}{(3.89s+1)(18.8s+1)} \end{bmatrix} \tag{4}$$

and

$$\hat{G}_d(s) = \begin{bmatrix} G_{d11} & G_{d12} \\ G_{d21} & G_{d22} \\ G_{d31} & G_{d32} \end{bmatrix} = \begin{bmatrix} \frac{0.14e^{-12s}}{6.2s+1} & \frac{-0.0011(26.32s+1)e^{-2.66s}}{(7.85s+1)(4.63s+1)} \\ \frac{0.53e^{-10.5s}}{6.9s+1} & \frac{-0.0032(19.62s+1)e^{-3.44s}}{(7.29s+1)(8.94s+1)} \\ \frac{-11.54e^{-0.6s}}{7.01s+1} & \frac{0.32e^{-2.6s}}{7.76s+1} \end{bmatrix} \tag{5}$$

2.6 Scaling the System

In order to perform a controllability analysis on the system, the system had to be scaled according to the method described in Skogestad & Postlethwaite (2001).

In order to perform the scaling operation, the upper and lower limits of all the variables have to be defined. The initial boundary values of all system variables are summarized in Table 2, Table 3, and Table 4.

Table 2: The boundaries of the manipulated variables in the system.

Manipulated Variable	**Lower Constraint**	**Upper Constraint**	**Steady State Value**
u_1, Reflux Flow Rate	0.068	0.245	0.18
u_2, Side Stream Flow Rate	0.00694	0.1	0.046
u_3, Reboiler Steam Pressure	15.6	34	20

Table 3: The boundaries of the controlled variables in the system.

Controlled Variable	**Maximum Set Point Change**	**Steady State Value**
y_1, Overhead Mole Fraction Ethanol	0.05	0.7
y_2, Side Stream Mole Fraction Ethanol	0.1	0.52
y_3, Temperature on Tray #19	8	92

Table 4: The boundaries of the disturbance variables in the system.

Disturbance Variable	**Lower Constraint**	**Upper Constraint**	**Steady State Value**
d1, Feed Flow Rate	0.6	1.1	0.8
d2, Feed Temperature	50	102	78

Using the information above the following matrices can be deduced, that will be used to scale the system

$$D_e = \begin{bmatrix} 0.01 & 0 & 0 \\ 0 & 0.01 & 0 \\ 0 & 0 & 4 \end{bmatrix} \tag{6}$$

$$D_u = \begin{bmatrix} 0.065 & 0 & 0 \\ 0 & 0.03906 & 0 \\ 0 & 0 & 4.4 \end{bmatrix} \tag{7}$$

$$D_d = \begin{bmatrix} 0.3 & 0 \\ 0 & 28 \end{bmatrix} \tag{8}$$

$$r = \begin{bmatrix} 0.05 & 0 & 0 \\ 0 & 0.1 & 0 \\ 0 & 0 & 8 \end{bmatrix} \tag{9}$$

Using the above matrices, the scaled system can be calculated using the following equations from Skogestad & Postlethwaite (2001),

$$G = D_e^{-1} \hat{G} D_u \tag{10}$$

$$G_d = D_e^{-1} \hat{G}_d D_d \tag{11}$$

From Equation 10 and Equation 11, the scaled system can be written as

$$G(s) = \begin{bmatrix} G_{11} & G_{12} & G_{13} \\ G_{21} & G_{22} & G_{23} \\ G_{31} & G_{32} & G_{33} \end{bmatrix} = \begin{bmatrix} \frac{4.29e^{-2.6s}}{6.7s+1} & \frac{-2.38266e^{-3.5s}}{8.64s+1} & \frac{-2.156e^{-s}}{9.06s+1} \\ \frac{7.215e^{-6.5s}}{3.25s+1} & \frac{-9.21816e^{-3s}}{5.0s+1} & \frac{-2.156e^{-1.2s}}{7.09s+1} \\ \frac{-0.56355e^{-9.2s}}{8.15s+1} & \frac{0.451143e^{-9.4s}}{10.9s+1} & \frac{1.1(10.1007s+0.87)e^{-s}}{(3.89s+1)(18.8s+1)} \end{bmatrix} \tag{12}$$

and

$$G_d(s) = \begin{bmatrix} G_{d11} & G_{d12} \\ G_{d21} & G_{d22} \\ G_{d31} & G_{d32} \end{bmatrix} = \begin{bmatrix} \frac{4.2e^{-12s}}{6.2s+1} & \frac{-2800(0.028952s+0.0011)e^{-2.66s}}{(7.85s+1)(4.63s+1)} \\ \frac{15.9e^{-10.5s}}{6.9s+1} & \frac{-2800(-0.062784s+0.0032)e^{-3.44s}}{(7.29s+1)(8.94s+1)} \\ \frac{-0.8655e^{-0.6s}}{7.01s+1} & \frac{2.24e^{-2.6s}}{7.76s+1} \end{bmatrix} \tag{13}$$

with

$$R = \begin{bmatrix} 5 & 0 & 0 \\ 0 & 10 & 0 \\ 0 & 0 & 2 \end{bmatrix} \tag{14}$$

3 Controllability Analysis

A full controllability analysis was performed on the system to establish whether:

1. The system has acceptable set point tracking characteristics.
2. The system has acceptable disturbance rejection characteristics.

The method used is described in Skogestad & Postlethwaite (2001).

3.1 Minimal Realisation of the System

The system written in the transfer function notation is in no danger of not being a minimal realizable system. It is only when the system is converted to state space notation that it runs the risk of not being a minimal realization.

When converting the transfer function model to a state space realisation of the system, it has to be noted that all dead time that is inherent to the system is ignored, as state space realizations cannot deal with dead time. The system was therefore never converted into its state space counterpart, as there are other techniques for calculating the system poles and zeros from Laplace domain notation.

3.2 Functional Controllability

The system has to be checked for functional controllability. This implies that outputs should be able to be controlled independently. There are two factors that have to be considered when checking for functional controllability of a system, namely

1. There have to be at least as many inputs as there are outputs
2. The rank of $G(s)$ should be greater than the number of outputs.

For consideration 1, mentioned above, the number of inputs and outputs in the system are equal. This criteria is therefore satisfied by the system.

For consideration 2, the minimum singular value (or $\underline{\sigma}$) of $G(j\omega)$ should be non-zero. In order to determine whether the system satisfies this criteria, all the singular values, of all

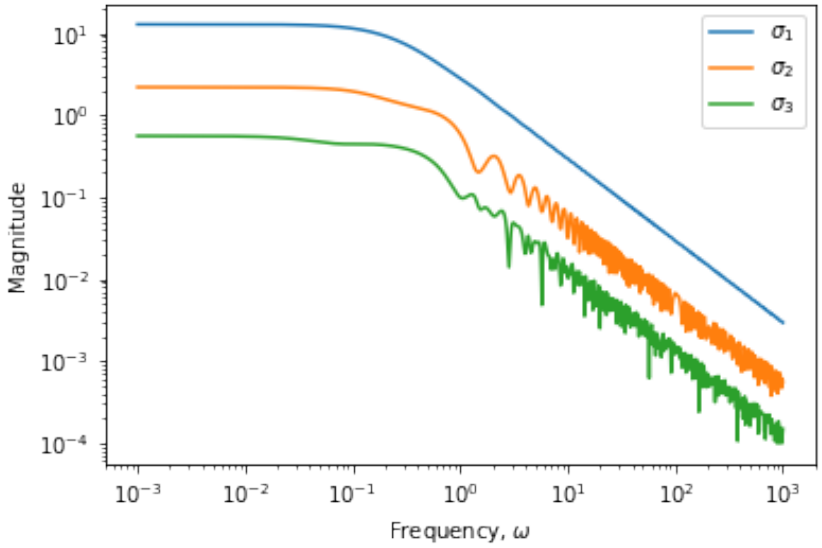

Figure 5: The singular values of $G(j\omega)$.

the outputs were computed of a wide frequency range. A bode diagram displaying the result can be seem in Figure 5.

As is clear from Figure 5, $\underline{\sigma}$ never reaches zero, although it does approach zero as the frequency goes to infinity.

Based on the above information, it can be concluded that the system is indeed functionally controllable. This implies that the system's rank is equal to the amount of outputs that the system has.

The current selected inputs and outputs can therefore be controlled with adequate independence. This further implies that outputs can return a response by some combination of the input variables.

A system that is functionally uncontrollable will have output responses remaining zero, whenever any combination of an input step function is applied to the system. This therefore results in an output that can in no way be controlled by the inputs, as the inputs do not effect the outputs at all. This however is not the case with the system being investigated.

3.3 System Poles

3.3.1 Calculating the System Poles

The poles of the system was calculated. The system has a total number of 25 poles. Some of the poles calculated are listed in Table 5. These only contain the more interesting poles. Please refer to Figure 6 for the locations of all the calculated poles.

Table 5: The poles of the system.

Pole	Real Part	Imaginary Part
p_1	-0.31	0
p_2	-0.26	0
p_3	-0.20	0
p_4	-0.23	0
p_5	0.036	0.23
p_6	0.036	-0.23

3.3.2 Calculating the System Pole Directions

The pole directions of the system was calculated by substituting the relevant pole values into $G(s)$ and calculating the input and output directions from the singular value decomposition. This was only done for the poles occurring in the Right Hand Plane (RHP). The calculated pole directions are listed in Table 6. Table 7 displays the same pole values in a more convenient notation (phasor notation). Using this notation the magnitude and phase shift of the input and output directions can be analysed for the specific pole frequency.

Table 6: The pole directions of the system.

Pole	Input Direction (V)	Output Direction (U)
p_5	$\begin{bmatrix} -0.71 \\ 0.68 + 0.12j \\ 0.13 + 0.05j \end{bmatrix}$	$\begin{bmatrix} -0.19 + 0.22j \\ -0.79 + 0.53j \\ 0.02 - 0.03j \end{bmatrix}$
p_6	$\begin{bmatrix} -0.71 \\ 0.68 - 0.12j \\ 0.13 - 0.05j \end{bmatrix}$	$\begin{bmatrix} -0.19 - 0.22j \\ -0.79 + 0.53j \\ 0.02 - 0.03j \end{bmatrix}$

Table 7: The pole directions of the system in phasor notation.

Pole	Input Direction (V)	Output Direction (U)
p_5	$\begin{bmatrix} 0.71 \\ 0.69\angle 10.1^\circ \\ 0.13\angle 19.6^\circ \end{bmatrix}$	$\begin{bmatrix} 0.29\angle 130.9^\circ \\ 0.96\angle 146.0^\circ \\ 0.04\angle -48.9^\circ \end{bmatrix}$
p_6	$\begin{bmatrix} 0.71 \\ 0.69\angle -10.1^\circ \\ 0.13\angle -19.6^\circ \end{bmatrix}$	$\begin{bmatrix} 0.29\angle -130.9^\circ \\ 0.96\angle -146.0^\circ \\ 0.04\angle 48.9^\circ \end{bmatrix}$

3.3.3 Discussion of System Poles

Most of the calculated system poles are in the open left hand plane (LHP). There is one pair of complex poles that lie in the open RHP. These poles will cause instability when they are approached. To gain better understanding into the what causes the system to behave in this way, the pole directions were calculated in Section 3.3.2.

Using Table 7 as reference, the directions of the system in this unstable condition can be analysed. From the table it is clear that the unstable response exists whenever the variable y_2 (side stream composition) is increased by almost one unit. This cannot be done without effecting the output y_1, as it is increased by almost a third of a unit during this response. Only the temperature can remain relatively unaffected during the response. We also note that y_1 and y_2 are in phase with one another, while y_3 is out of phase with the first two outputs.

Looking at the input directions in Table 7, it is clear that the described output is obtained from manipulation of u_1 and u_2. While u_3 is manipulated slightly, its amplitude is well below the amplitude of the other system inputs. We can therefore generalize and say that the pole exists when reflux flow rate is increased and the side stream draw off flow rate is decreased by the same amount. One small thing to note is that the input u_1 does not have a phasor notation, as it is not a complex variable.

From the above it is clear, that the side stream composition cannot be stepped one unit by manipulating the side stream flow rate and reflux flow rate exclusively. This step response in composition will have to be obtained from other combinations of measured variables for the system to remain stable.

From a production point of view, this will not likely pose to be problem, as it is not a scenario that is very likely to exist. As mentioned earlier, the main ethanol product is in the distillate of the column. The shift described by this pole, will decrease both the

distillate and side stream flow rates, resulting in a plummeting production profit as the product streams are redirected to waste or downstream processing (the bottoms flow). Special care should therefore be taken when designing the controller algorithm to steer clean from this control scenario.

An easier, more intuitive, way to obtain the same results (of adjusting the composition of the side stream) will be to only manipulate the side stream flow rate while increasing the temperature of the bottom plate. This will leave the production flow rate of the distillate relatively unaltered, while side stream flow rate will be sacrificed for composition. Note that this result can easily be obtained by using a decentralized controller.

3.4 System Zeros

3.4.1 Calculating the System Zeros

The system zeros were calculated. The system contains a total number of nine zeros, all of them located in the left hand plane (LHP). The system zeros are given in Table 8.

Table 8: The zeros of the system.

Zero	Real Part	Imaginary Part
z_1	-0.3077	0
z_2	-0.2571	0
z_3	-0.2	0
z_4	-0.1493	0
z_5	-0.1227	0
z_6	-0.1157	0
z_7	-0.1104	0
z_8	-0.0917	0
z_9	-0.0532	0

Since all zeros are in the LHP, and will in no way cause limitations on the bandwidth or stability of the system, the directions of the zeros were not calculated.

3.4.2 Discussion of System Zeros

The system zeros exists for values of s where the system $G(s)$ loses rank. The zeros calculated, are transmission zeros of the system as they do not relate to the zeros of the

elements that make up the transfer function matrix $G(s)$. It is clear that there are no RHP zeros, and no further analysis of the zeros is required, as there are no limitations imposed by Left Hand Plane (LHP) zeros.

LHP zeros will mostly cause high overshoots during control, but this does not pose as a stability concern for the system and will in no way limit the bandwidth of the system.

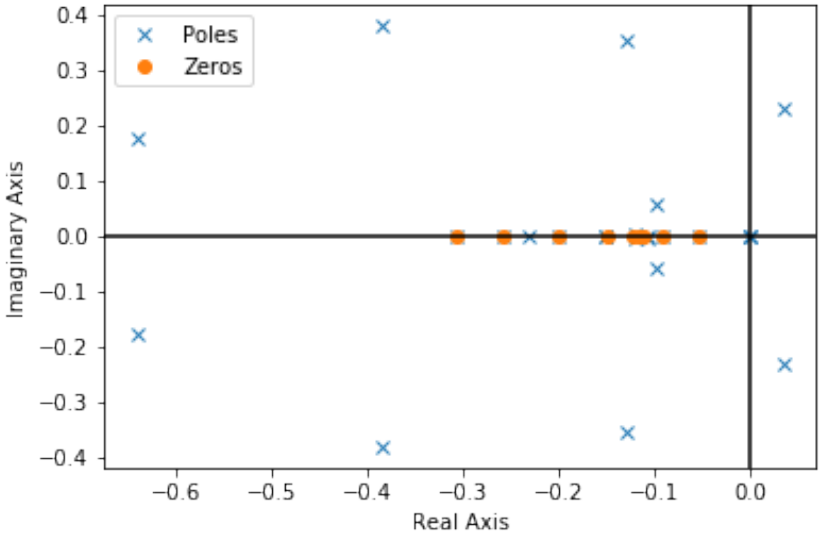

Figure 6: A graphical representation of the system's poles and zeros.

3.5 RGA Values of the System

The Routh Gain Array (RGA) of $G(j\omega)$ was calculated, for all values of ω, where the frequency domain analysis held stable. This enables the analysis of RGA values not only at the crossover frequencies, but at all other frequencies to thoroughly check for large RGA elements that will render a plant that is difficult to control. Due to dead time in the system, the frequency response of the RGA calculation tends to become severely unstable at higher frequencies. Luckily, spikes in the response will always tend to go downward, and the maximum RGA values can still be calculated.

The frequency at which RGA analysis breaks down is $\omega = 0.2$. Al that can be said about this it that the correct functioning of a decentralized controller cannot be predicted above this frequency. This is due to the effects that multiple delays have on the system. The calculated RGA values can be seen in Figure 7.

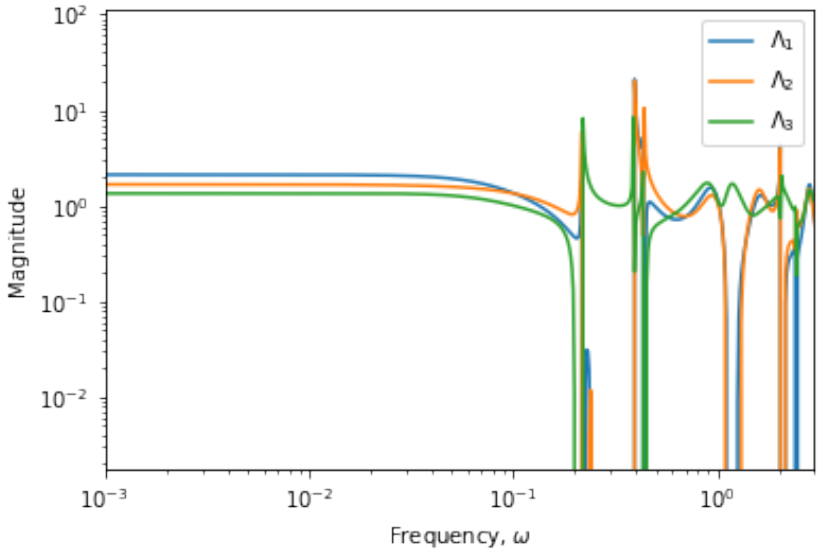

Figure 7: The diagonal values of RGA matrix, Λ, over a wide range of frequencies.

To verify that the off-diagonal values remain within acceptable ranges, the RGA of $G(0)$ and $G(j\omega)$ with $\omega = 10^{-1}$ was calculated. The two matrices calculated are

$$\Lambda G(0) = \begin{bmatrix} 2.11 & -0.84 & -0.26 \\ -0.59 & 1.67 & -0.08 \\ -0.52 & 0.17 & 1.34 \end{bmatrix} \tag{15}$$

$$\Lambda G(j10^{-1}) = \begin{bmatrix} 1.36 & -0.33 & -0.03 \\ -0.37 & 1.34 & -0.03 \\ 0.02 & -0.02 & 1.00 \end{bmatrix} \tag{16}$$

From the values described above, it is not unreasonable to state that a decentralized controller can be implemented on site. This is the configuration of the proposed control scheme, and based on the RGA values this will be beneficial. Interestingly, in Section 3.7 the delays of the elements along the diagonal of $G(s)$ are the smallest compared to the off-diagonal elements. This further encourages the use of decentralized control on the plant.

3.6 Singular Values of the System

3.6.1 The Minimum Singular Value and Set-point Tracking

The minimum singular value is a useful tool when doing a controllability analysis. The minimum singular value for this system is depicted in Figure 5.

The minimum singular value should be as large as possible, especially at frequencies where control is needed (Skogestad & Postlethwaite, 2001).

From Figure‘5, it is clear that

$$\underline{\sigma}(G(j\omega)) < 1, \forall\omega \tag{17}$$

This implies that it is not possible to make output changes of unit magnitude, by using inputs of unit magnitude for any input direction of V.

This is bad from a controllability point of view, especially when considering set-point tracking. When tracking set-points, outputs ideally have to controlled by making single set-point changes. This enables the use of a decentralized controller. An example of such a controller (represented in a standard transfer function notation) is

$$K(s) = \begin{bmatrix} \frac{K_1}{\tau_1 s+1} & 0 & 0 \\ 0 & \frac{K_2}{\tau_2 s+1} & 0 \\ 0 & 0 & \frac{K_3}{\tau_3 s+1} \end{bmatrix} \tag{18}$$

With the current plant configuration and design, the use of a decentralized controller is possible, but acceptable set-point tracking will not be possible as the outputs will not reach the set-points on the high and/or low set-point values.

For example; when the temperature on tray # 19 , y_3, is controlled between 88 and 96 °C, set-point tracking by manipulation of the stream feed pressure, u_3, will be acceptable (when considering a decentralized controller that contains an integral component). Acceptable set-point tracking includes: fast response time, elimination of error, and robust responses. An adequately fast response time for this system will be around 45 minutes. With a high enough gain value, K_{c3}, this will be achieved. The integral component of the controller will eliminate the error completely over time, given that the integral component of the controller, τ_{c3}, is large enough. Robust control will be achieved by tuning the controller values after initial implementation.

Now, when considering set-points on the outer limits of the control range for y_3, the control system will not perform acceptably. For instance when the set-point of y_3 is set to ranges 84 to 88 °C or 96 to 100 °C, the response time of the set-point change may still be good, but the error will not be able to be cancelled. This is due to the minimum singular value of the system being smaller than 1. The unit change in the input, u_3, will not cause a unit change in the output, y_3. Since the system is scaled, this simply means that the outer set-points cannot be reached by manipulating one set of input variables (with different magnitudes and directions).

The situation discussed above, only applies to the y_3 and u_3 control pairing. From Figure 5, it is clear that the criteria stated in Equation 17 is satisfied for the y_2 and u_2 paring for all frequencies where $\omega < 0.28$. Similarly, the criteria in Equation 17 is satisfied in the y_1 and u_1 pairing for all frequencies where $\omega < 2.97$.

There are a few options for improvement and successful implementation of the control system. They are

1. To implement a controller that is not decentralised. This controller can still control y_1 an y_2 using u_1 and u_2. y_3 will then be controlled by a combination of u_3 and u_2 (this follows from the RGA matrix analysis, where u_1 is negative with regard to y_3). The controller equation will then take the form of

$$K(s) = \begin{bmatrix} \frac{K_1}{\tau_1 s+1} & 0 & 0 \\ 0 & \frac{K_2}{\tau_2 s+1} & 0 \\ 0 & \frac{K_{3_1}}{\tau_{3_1} s+1} & \frac{K_{3_2}}{\tau_{3_2} s+1} \end{bmatrix} \tag{19}$$

   While this will ensure that acceptable set-point tracking of the bottom tray temperature is accomplished, there will be a loss in the performance and robustness of the control in the side-stream composition.

2. Increase the size of the control valves controlling the stream pressure. This will increase the overall gain in the system, shifting the singular values in an upward direction. This will render acceptable set-point tracking of all parameters.

3. Lower the required range wherein set-point tracking has to be performed.

More insight into the problem is gained when the different singular value directions are analysed.

3.6.2 Singular Value Directions

The directions of the singular values are used to gain better understanding into how the three outputs are responsible for the overall system gain. The directions are calculated at both low and high frequencies to analyse the behaviour across a wide range of frequencies. The two frequencies selected are $\omega = 0$ for low frequncies (or steady state conditions), and $\omega = 1$, which is the frequency at which the delays in the system causes the singular value to oscillate. The SVD for the low gain value is calculated as

$$G(0) = \underbrace{\begin{bmatrix} -0.38 & 0.88 & 0.26 \\ -0.92 & -0.39 & -0.03 \\ 0.07 & -0.25 & 0.96 \end{bmatrix}}_{U} \underbrace{\begin{bmatrix} 12.9 & 0 & 0 \\ 0 & 2.21 & 0 \\ 0 & 0 & 0.56 \end{bmatrix}}_{\Sigma} \underbrace{\begin{bmatrix} -0.64 & 0.51 & 0.57 \\ 0.73 & 0.62 & 0.23 \\ 0.22 & -0.59 & 0.77 \end{bmatrix}}_{V^H} \tag{20}$$

while the SVD for the higher gain is

$$U(G(1j)) = \begin{bmatrix} 0.17\angle 152^\circ & 0.96\angle -74.3^\circ & 0.22\angle 116^\circ \\ 0.98\angle -86.4^\circ & 0.15\angle -132^\circ & 0.02\angle 58.3^\circ \\ 0.0\angle -30.1^\circ & 0.23\angle 100^\circ & 0.97\angle 111^\circ \end{bmatrix} \tag{21}$$

$$\Sigma(G(1j)) = \begin{bmatrix} 2.83 & 0 & 0 \\ 0 & 0.59 & 0 \\ 0 & 0 & 0.10 \end{bmatrix} \tag{22}$$

$$V^H(G(1j)) = \begin{bmatrix} 0.77\angle 0.0^\circ & 0.58\angle -180^\circ & 0.25\angle 0.0^\circ \\ 0.63\angle -17.2^\circ & 0.65\angle -18.3^\circ & 0.41\angle 166^\circ \\ 0.07\angle -134^\circ & 0.47\angle -121^\circ & 0.87\angle -117^\circ \end{bmatrix} \tag{23}$$

From the above it is clear that

1. The high process gain at low frequencies is achieved by manipulation of variables u_1 and u_2 in opposite directions. This does check out with the process (when considering steady state conditions), as changing the reflux and side stream flow rates will most definitely cause the greatest upset to the process. It is clear that y_2 will be most effected by this input direction, while y_1 will be moderately effected. As is also expected, y_3 will remain relatively unchanged, as the changes in reflux and

side stream flow rates will not greatly effect the bottoms flow rate (and therefore the temperature on the bottom tray).

2. Moving to high frequencies the exact same phenomenon is seen as described in the point above. The magnitude of input and output directions are nearly identical. Interestingly enough the inputs causing the high gain are slightly out of phase, but where outputs y_1 and y_2 are severely out of phase with one another. The output direction also points more to the direction of y_2 as the frequency is increased.

3. The low process gain at low and high frequencies is caused by an input of all three input variables in the same direction (at higher frequencies the variables are neatly space out i.t.o their phases). The variables have varying magnitudes, but the magnitude of u_3 is clearly the biggest in both scenarios. When analysing the output directions, it is clear that the low gain condition is achieved when y_3 is manipulated while keeping the other two output variables constant. This is also the case for both low and high frequency low gain conditions. The outputs in the low gain condition are in phase with one another.

4. There is no big change in the directions of the inputs and outputs between the low and high frequencies. This is beneficial for control, as shifts in the input variables will deliver consistent results with regard to high and low overall process gains.

5. To generalize, high overall gains are obtained when adjusting variables u_1 and u_2 simultaneously, in order to change variable y_2. This should be compared to the RHP pole calculated in Section 3.3.2. It is clear that the RHP pole is obtained when the process is shifted to reach its highest possible overall gain. This is not ideal, as we would like to utilize the high gain directions to speed up response times and increase performance. In this case performance will have to be sacrificed to obtain stable responses. Inputs that are in phase seem to favour high gain conditions, while outputs that are in phase tend to favour low gain condition. The low gain condition involves the change of temperature in the column.

3.7 System Bandwidth

The bandwidth of the system is the maximum frequency where sensible control can still be implemented. Mathematically it is where the sensitivity function of the system first crosses $\frac{1}{/}\sqrt{2}$, or

$$|S(j\omega)| = \frac{1}{\sqrt{2}} \tag{24}$$

Since no controller is implemented as yet, there is no way of calculating the sensitivity function. As discussed in Section 3.3 and Section 3.4, there are no Right Hand Plane (RHP) zeros in this system, and therefore there is no bandwidth limitations imposed by zeros. There are two RHP poles present, that will impose limitatiosn on the system. The limitatios imposed on the system include

1. Limitations on the input usage. This constrains the amount of gain that can be applied to the system with a controller. In general

$$||KS||_\infty \geq ||u_p^H G_s(p)^{-1}||_2 \tag{25}$$

   This is not entirely relevant to this report, as it entails the implementation of a controller. While this upper bound may be useful to assist with the design of the controller, the main focus of this report will remain on the controllability of the system.

2. Limitations on the bandwidth. In short, the system has to react fast enough to avoid running into stability problems. The RHP pole therefore gives a maximum bound on the bandwidth. According to Skogestad & Postlethwaite (2001) the minimum closed loop bandwidth is

$$\omega_B \geq 2|p| \tag{26}$$

   Using the equation the minimum bandwidth can be calculate to be $\omega_B = 0.46$. This gives a response time of less than 2.15 minutes.

The system also contains a lot of dead time. There is dead time in each transfer function, as this is it is inherent to the fitting function used to build the model. There are constraints on the bandwidth due to this dead time. To visualize the dead time inherent to the system, please refer to Equation 27. This equation, simply named the dead time matrix, is a representation of the dead time elements (θ_{ij}) for the respective transfer functions.

$$\Theta = \begin{bmatrix} 2.6 & 6.5 & 9.2 \\ 3.5 & 3.0 & 9.4 \\ 1.0 & 1.2 & 1.0 \end{bmatrix} \tag{27}$$

The lower bound time delay for each output (or contained within each row of Θ) is of interest. This is because the minimum time for any input to effect the relevant output

(θ_i^{min}), can be seen as the delay that is pinned to output y_i. Alternatively this statement can be represented mathematically as

$$\theta_i^{min} = \min_j \theta_{ij} \tag{28}$$

The bandwidth of input u_i is then limited by the lower bound $1/\theta_i$. Table 9, contains a summary of the bandwidth limitations of the system.

Input	**Theta**	**Bandwidth**
y_1	2.6	0.38
y_2	3.0	0.33
y_3	1.0	1.0

Table 9: Bandwidth limitations imposed by time delays.

While these limitations are in no way ideal, they do not pose to be a major threat for the control of the system. There are a few conclusions that can be drawn from this, namely

1. When looking at Equation 27 together with Section 3.5, it is clear that the diagonal elements that are paired in the RGA matrix, also contain the least amount of dead time. This is good, as it is obvious that you want to control a variable with an input that does not take long to effect the variable. Pairing of the variables are therefore made relatively straight forward.

2. The delays imposed are not that significant when considering the desired response times for the control system. Required response times for the variables of the distillation column range between 30 and 60 minutes. The maximum delay calculated here (3 minutes), is relatively small and a low gain controller should be able to control the system with adequate performance. The performance of the system is discussed in more detail later in the report (Section 6).

3. Controlled variables y_1 and y_2 are more constrained by the RHP pole that exist than the delay that is inherent to these variables. Only y_3 is limited by the delay of the response. This is expected as the pole clearly influences y_1 and y_2 the most (Table 6). y_3 also has the least amount of dead time, shortening the period wherein reasonable control can be expected.

3.8 Disturbance Rejection

In order for the system to successfully reject disturbances, tight control and large bandwidths are required to reject disturbances when disturbances are large or "fast".

To evaluate a MIMO system's ability to reject disturbances, the disturbance directions have to be evaluated (which is not the case when considering a SISO system).

The model contains two disturbances, each having it's own associated direction. The disturbance directions are defined as

$$y_d = \frac{1}{||g_d||_2} g_d \tag{29}$$

where g_d represents the effect of a single disturbance on the outputs ($y = g_d d$).

The disturbance directions for both disturbances were evaluated for all frequencies. The results can be seem in Figure 8.

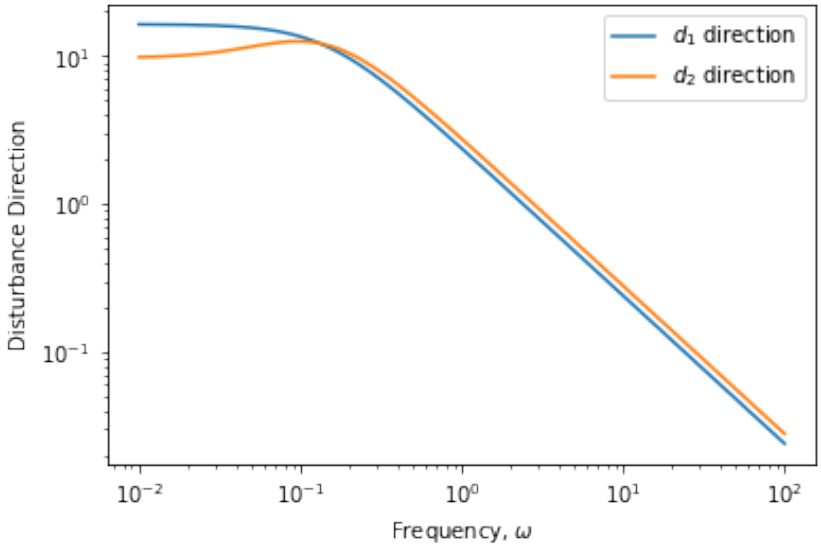

Figure 8: The disturbance directions as a function of frequency.

Now, following that the system has been scaled (Section 2.6), we can say that the worst-case disturbance to be selected is $|d_i(\omega)| = 1$. Using this, and the fact that with feedback control we have $e = Sg_d d$, the disturbance performance objectives are then satisfied when

$$||Sg_d||_\infty < 1 \tag{30}$$

Note that $S(s)$ could not actually be calculated. This is because no controller has yet been designed for the system. To gain better understanding of the disturbances in the system, a proportional decentralized controller with a gain of 1 (for all elemnts) was used.

Skogestad & Postlethwaite (2001) used the above and derived tight bounds on the sensitivity function and loop gain for MIMO system, considering the disturbance directions as well. For the system to adequately reject disturbances, we at least require that

$$\underline{\sigma}(S) < \frac{1}{||g_d||_2} \tag{31}$$

Where S is the sensitivity function of the transfer function model, or can be given mathematically as

$$S = (I + G)^{-1} \tag{32}$$

for a negative feedback loop.

Equation 31 can be represented graphically. The left-hand side and right-hand side of the equation was plotted for all values of ω. The results are displayed in Figure 9.

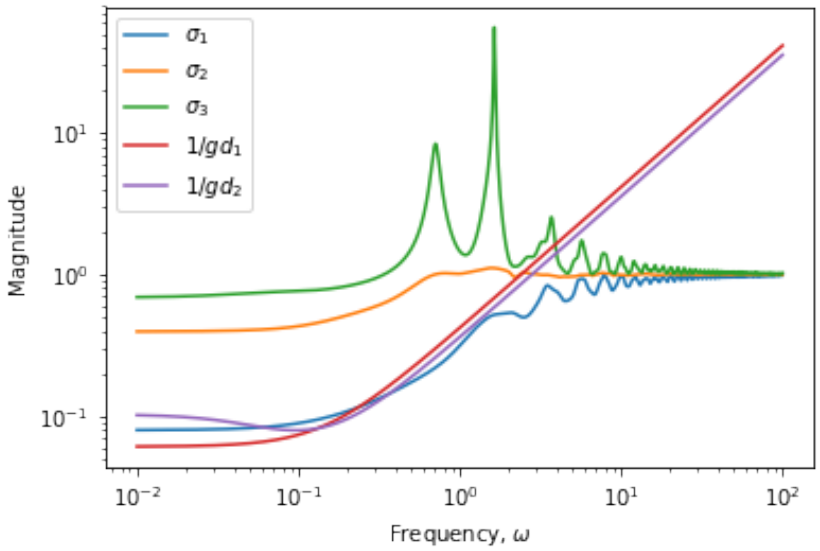

Figure 9: The disturbance directions with respect to the singular values of the sensitivity of $G(s)$, $S(s)$.

From Figure 9, it is clear that, based on the criteria stated in Equation 31, there may be some problems regarding disturbance rejection (especially at low frequencies). To share more light on the causes of the problem, an more in depth analysis is conducted below.

3.9 Disturbances and Input Saturation

3.9.1 Analysis for Perfect Control

Here it is asked whether disturbance rejection is possible, without input saturation ($||u|| < 1$). There are two methods of evaluating this, by use of

1. The max-norm.
2. The two norm.

As the system is square, the max-norm can be used to analyse this plant. Disturbances are analysed separately, and combined to gain full understanding of how the disturbances will effect the controller input.

When considering single disturbances, input saturation is avoided (and perfect control is achieved) when

$$||G^{-1}g_d||_{max} < 1 \tag{33}$$

and when considering simultaneous disturbances the requirement can be rewritten to

$$||G^{-1}G_d||_{i\infty} < 1 \tag{34}$$

where $||\cdot||_{i\infty}$ is the induced max-norm defined as

$$||A||_{i\infty} = \max_j \Big(\sum_i |a_{ij}| \Big) \tag{35}$$

The criteria stated above is displayed in Figure 10.

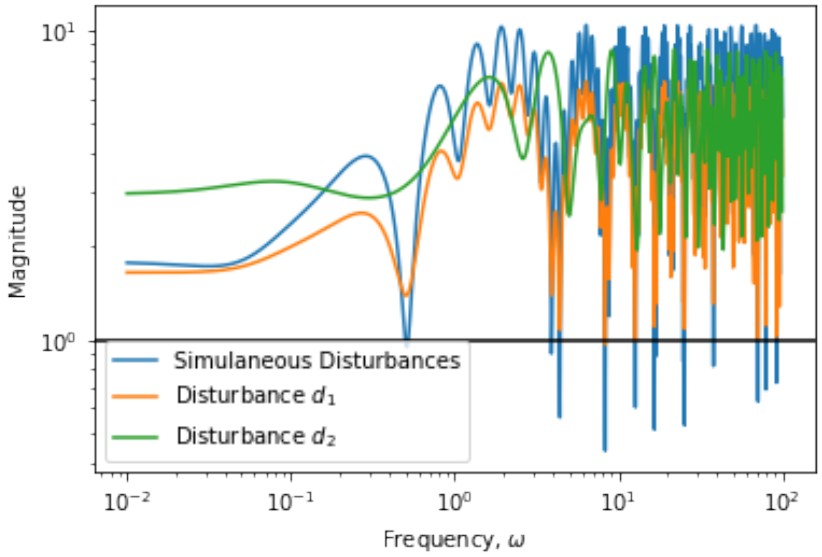

Figure 10: The effect of disturbances on input saturation.

From Figure 10, it is clear that perfect control is not possible for either disturbance, or even for a combination of both. The disturbance d_2 is the most problematic, as the disturbance causes $||G^{-1}g_d||_\infty||$ to be greater than 1 for all values of frequency. Perfect control of this disturbance is not possible.

Input saturation is therefore unavoidable. This does not necessarily mean that the plant is uncontrollable with regard to disturbance rejection. An analysis for acceptable disturbance rejection with regard to input saturation has to be performed.

3.9.2 Analysis for Acceptable Control

Acceptable control exists when, for the response $e = Gu + G_d d$ it is possible achieve $||r|| \leq 1$ for any $||d|| \leq 1$ using inputs $||u|| \leq 1$. Only the max-norm is used in this section. The conditions resulting from the analysis are for achieving $||e|| \leq 1$ (the minimum requirement).

The criteria derived by Skogestad & Postlethwaite (2001) for system to exhibit acceptable control characteristics is given as

$$\sigma_i(G) \geq |u_i^H g_d| - 1, \text{ at frequencies where } |u_i^H g_d| > 1 \tag{36}$$

Figure 11, Figure 12 and Figure 13 are the graphical representations of the criteria stated in Equation 36 for the three different input directions. The effect of both disturbances

are plotted against the singular value for the specific input. This will help to gain insight into the way that disturbances effect the input values to the controller.

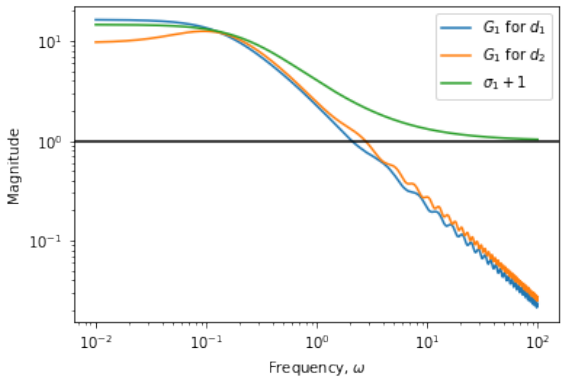

Figure 11: Graphical representation of criteria outlined in Equation 36, for e_1

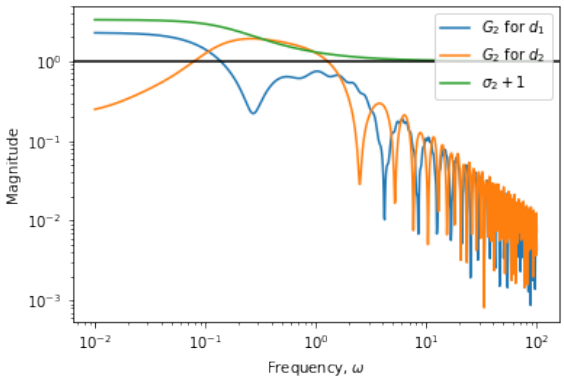

Figure 12: Graphical representation of criteria outlined in Equation 36, for e_2

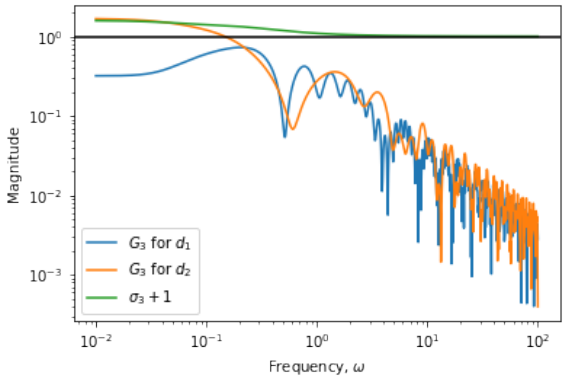

Figure 13: Graphical representation of criteria outlined in Equation 36, for e_3

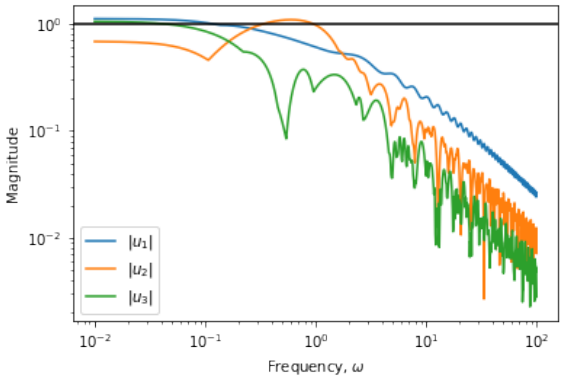

Figure 14: The required controller input values for the worst case

When considering Figure 11, it is clear that the input into the controller (controlling y_1) is saturated at low frequencies. This is due to the effects that d_1 has on the system. It is clear that a maximum change in the feed flow rate, will result in the reflux flow rate being saturated. This translates to a fully open or fully closed control valve in this section of the plant. There are two solutions to the problem, namely

1. Install a bigger control valve (and therefore line size) on the reflux stream. This change will impact the mathematical model by changing the gain and response times in the first row of transfer function matrix $G(s)$. This will speed up the dynamics of the system, and result in higher minimum singular values for $S(s)$,

especially at low frequencies where the problem is experienced. Better disturbance rejection will result.

2. Lower the maximum designed for disturbance size. This can be done by tighter control upstream from the distillation column (by the flow regulator/controller indicated in Figure 2).

Both actions will take considerable time to implement, as the effect of tighter flow control will effect the reactor vessel's control as well. A bigger, or more sophisticated control valve, will have a installation cost, as well as a downtime, as well as recommissioning of the system, production cost implication.

From Figure 12 it is clear that acceptable control is possible, since the second input to the controller is saturated by neither disturbance changes (for all frequencies).

Regarding Figure 13, it is clear that disturbance rejection is again not acceptable, as the third input to the controller (e_3) is saturated when disturbance d_2 is at it's maximum feed value. When relating back to the physical process, this means that the stream pressure control valve, fully closes when the feed temperature rises to 106 °F or fully opens when the feed temperature drops to 58 °F. To solve this problem there again exists a few solutions, namely

1. Increase the size of the control valve. When doing this, it is imperative that the compressors in the stream line's design also be reviewed, as it may be required that a higher stream flow rate be required at the lowest disturbance value. The major downside of this option, is that there is no compensation for when the feed temperature rises to the maximum disturbance value. Even the bigger control valve will still fully close.

2. Decrease the disturbance limit values. This is again the most straightforward method to increase the effectiveness of disturbance rejection over the distillation column. This can be done by implementing tighter control over the feed heat exchanger unit (indicated in Figure 2). Methods to implement tighter control will be to increase the controller gain of the unit (an decreasing the amount of integral control). Implementing a feed forward controller on the heat exchanger unit by adding the working fluid's temperature as measured variable is another option (although this will not be the most cost effective solution).

3. Change the controlled variable y_3. By changing the controlled variable y_3 from the temperature on tray #19, to the boil-up ratio will reduce the response time

in dynamics of the third row in $G(s)$. This will lead to higher singular values in $S(s)$, especially at low frequencies, and disturbance rejection performance criteria will be met. This solution has the downside that the bottoms composition will not be controlled directly. Since the production is more interested in the quality of the distillate composition (as this is where the ethanol product is), this is not a major loss and the solution can be considered. A full controllability analysis will have to be conducted on the new system if this is the chosen solution, as the dynamics of the whole MIMO transfer function model will change.

Figure 14 illustrates the required input variables (u_i) for maximum disturbance rejection. The figure reiterates the problems experienced in Figure 11 and Figure 13, where the inputs required for disturbance rejection will saturate the controller.

4 Changing the System Bounds

4.1 Disturbance Rejection and Input Saturation

This section will look at the proposed changes stated in Section 3.9.2. Since there is no information on the current controllers and final control elements employed on site, investigation into changes of the control hardware will not be conducted. This is purely due to

1. Lack of information about current control infrastructure.
2. Lack of a first principles mathematical model, or Aspen simulation where the sizes of the control elements can be changed at will without any additional cost.

The proposed changes to the perimeters of the control system will therefore be investigated. As mentioned in Section 3.9.2, disturbance rejection is required for a too high range of both disturbances. In order to rectify the situation, the ranges where adjusted. This in turn caused the scaled system to change, and new responses resulted. Table 10 contains more information with regard to the proposed ranges.

Table 10: The new proposed boundaries of the disturbance variables in the system.

Disturbance Variable	**Lower Constraint**	**Upper Constraint**	**Steady State Value**
d1, Feed Flow Rate	0.65	1.0	0.8
d2, Feed Temperature	60	95	78

This led to a new scaling matrix

$$D_d = \begin{bmatrix} 0.2 & 0 \\ 0 & 18 \end{bmatrix} \tag{37}$$

and a new disturbance matrix

$$G_d(s) = \begin{bmatrix} G_{d11} & G_{d12} \\ G_{d21} & G_{d22} \\ G_{d31} & G_{d32} \end{bmatrix} = \begin{bmatrix} \frac{2.8e^{-12s}}{6.2s+1} & \frac{-1800(0.028952s+0.0011)e^{-2.66s}}{(7.85s+1)(4.63s+1)} \\ \frac{10.6e^{-10.5s}}{6.9s+1} & \frac{-1800(-0.062784s+0.0032)e^{-3.44s}}{(7.29s+1)(8.94s+1)} \\ \frac{-0.577e^{-0.6s}}{7.01s+1} & \frac{1.44e^{-2.6s}}{7.76s+1} \end{bmatrix} \tag{38}$$

The same mathematical procedure is then followed as outlined in Section 3.9.2, to establish whether acceptable disturbance rejection can take place. The following figures result.

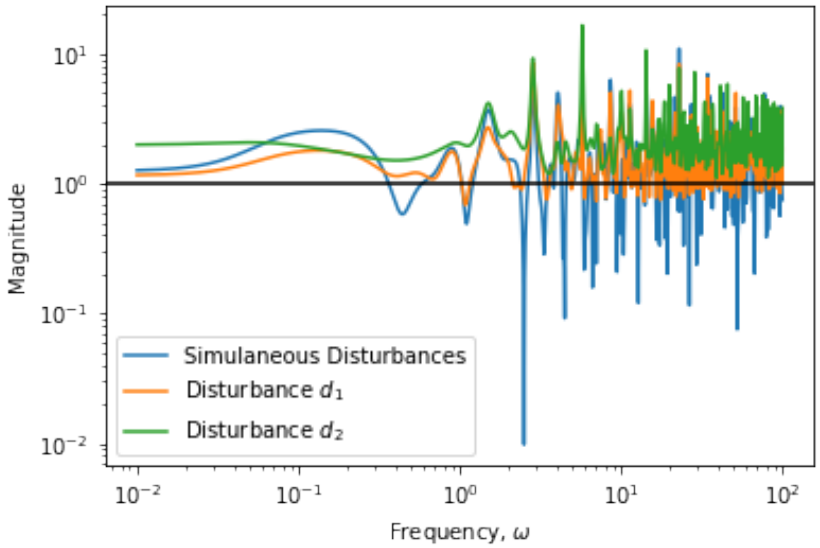

Figure 15: The effect of disturbances on input saturation.

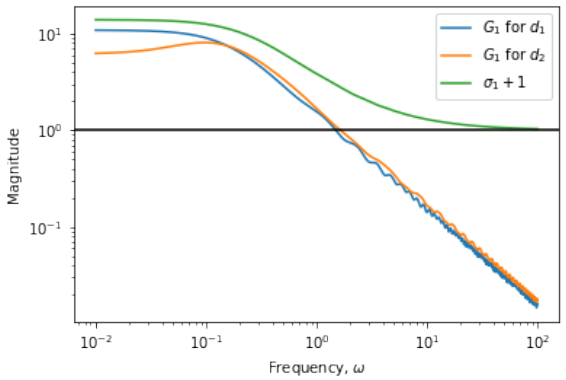

Figure 16: Graphical representation of criteria outlined in Equation 36, for e_1

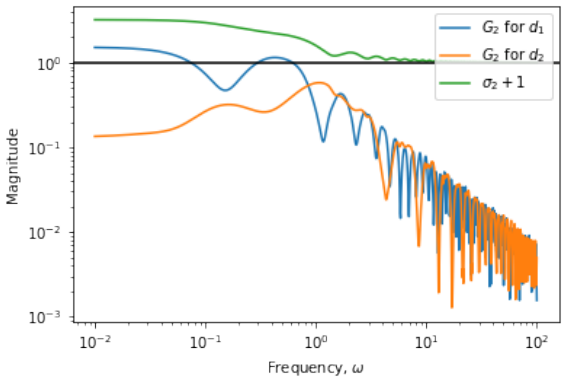

Figure 17: Graphical representation of criteria outlined in Equation 36, for e_2

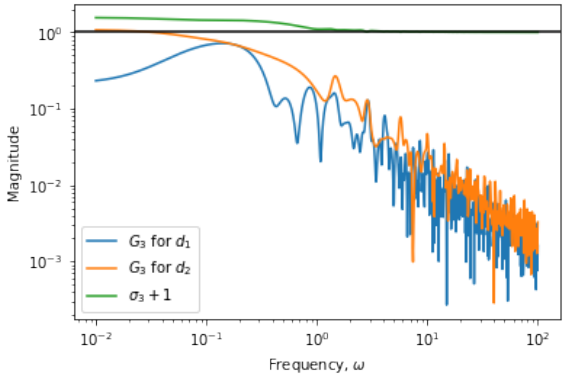

Figure 18: Graphical representation of criteria outlined in Equation 36, for e_3

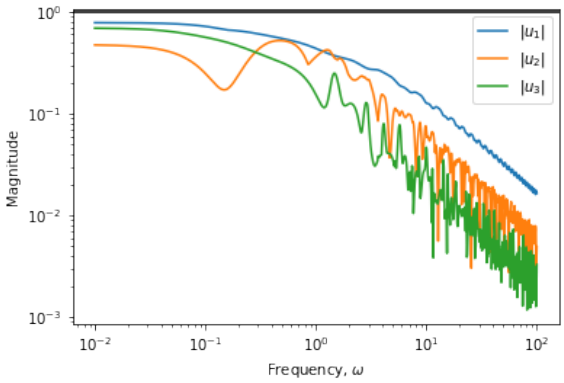

Figure 19: The required controller input values for the worst case

From the figures above the following is apparent:

1. Even with the reduced control system requirements, perfect control is not achievable (Figure 15).

2. Lowering the control bounds does however result in a system that can acceptably rejects all disturbances (Figure 16, Figure 17, Figure 18, and Figure 19.)

5 Uncertainty and Robustness

In this section the uncertainty model will be derived to include various aspects where uncertainly is present.

Looking at the method in which the model is derived, the main uncertainties in this description of the process are

1. Parametric uncertainty. This is from the fact that the model is fitted. The variables used for fitting the models were rounded to produce numbers that are easy to work with. This causes uncertainty regarding the accuracy of the model, as all the variables may be wrong by a fractional amount.
2. Uncertainty due to neglected dynamics. This will most certainly be included in the current model, as the core principle behind fitting dynamic models to experimental data involves the simplification of multi order differential equations to first or second order systems.

The above list contains the uncertainties that are certain. Some uncertainties are unlikely. These uncertainties will not be considered when deriving the uncertainty model. This includes

1. Neglected delays. This can be excluded, as all the modelled equations contains delays. The uncertainty regarding the delays will therefore only be analysed when looking at the parametric uncertainty of the values of θ_{ij}.

5.1 Choosing the Uncertainty Weight Form

A major thing to consider when setting up the uncertainty model is which uncertainty weight form to use. The two major weights to choose from are

1. Additive uncertainty.
2. Multiplicative weight uncertainty.

The major deciding factor for the choice will be the ease of fitting the uncertainty weight to the smallest uncertainty radius of all possible plants (Π). In mathematical terms the radius can be described as

$$l_A = \max_{G_p \epsilon \Pi} |G_p(j\omega) - G(j\omega)| \tag{39}$$

for additive uncertainty, and

$$l_I = \max_{G_p \epsilon \Pi} |\frac{G_p(j\omega) - G(j\omega)}{G(j\omega)}| \tag{40}$$

for multiplicative uncertainty. In the above equations $G_p(j\omega)$ refers to the perturbed model. The complete uncertainty analysis was pulled from Skogestad & Postlethwaite (2001), and for more information regarding the concepts please consult the reference material. Preferably the uncertainty weight should have the lowest possible order. The relative shape difference between the two uncertainty descriptions are displayed in Figure 20.

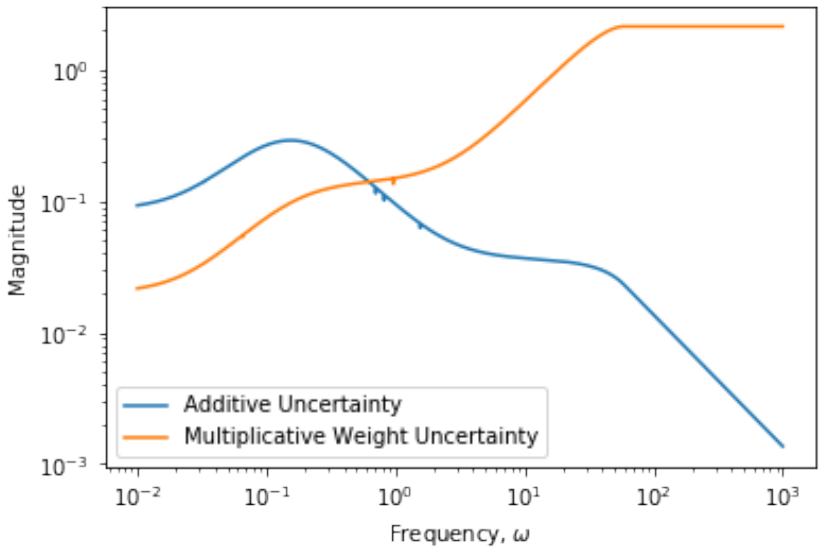

Figure 20: A comparison between additive and multiplicative uncertainty weight requirements, when analysing parametric uncertainty of a first order plus dead time equation.

From the picture it is clear that drastically different shapes for l_A and l_I is obtained using the uncertainty descriptions. When the two are compared, it is clear that

1. The additive uncertainty will require at least one lead and two lag term to get an acceptable fit. Only using one lag will lead to an over estimated uncertainty for

low frequencies. To gain an even tighter fit one additional lag and lead term can be added. This however will result in a very complex uncertainty weight.

2. The multiplicative uncertainty requires only one lag and one lead to get an acceptable fit. For a tighter fit, one additional lag and lead can be added. This is not entirely necessary, as the frequencies where uncertainty is over estimated are in the crossover frequency range. This is therefore a very conventional fit. In later sections the benefit of this estimation with regard to unmodelled dynamics uncertainty is discussed.

For this uncertainty description multiplicative weights will be used to describe the uncertainty. This is simply due to the ease of fitting the multiplicative weights to the uncertainty descriptions.

5.2 Parametric Uncertainty

As mentioned in the previous section, parametric uncertainty is inherent to the model. Using the data and subsequent models fit to the data, is was decided to

- Estimate the uncertainty of all gains as 2 %.
- Estimate the uncertainty of all time constants as 10 %.
- Estimate the uncertainty of all time delays as 2 %.

The values above are chosen based on the distribution of data points in key places, during the step test analysis. The steady state gains were relatively clear due to a small variance distribution of particles along the horizontal lines (steady state) in the time domain responses. The same principle applies to the time it takes before a response is observed. The critical point is quite easily identifiable, and the first order plus dead time models can capture the dead time in the system with little uncertainty regarding the value of the dead time. This is most definitely due to high quality measuring devices that can deliver consistent accurate measured values.

It is only in the middle of the step responses that a deviation in measured value occurred. This is captured in a lower local R^2 value in this region of the step response. This is the reason why the time constants are more uncertain than the other parameters.

All the first order plus dead time transfer functions within $G(s)$ have the relatively the same shape (their uncertainty descriptions are the same). For this reason, the same fitting function was used to describe the performance weights. This function is

$$w_{Ii} = \frac{Ts + k_1}{(T/2.5)s + 1} \tag{41}$$

This is the minimum order uncertainty weight that could be fit to the functions, and was chosen to simplify the uncertainty model. Table 11 contains all the various constants for the uncertainty model of $G(s)$.

Transfer Function	**Uncertainty Weight**	T	k_1
G_{11}	w_{I11}	0.7	0.02
G_{12}	w_{I12}	0.5	0.015
G_{13}	w_{I13}	0.55	0.04
G_{21}	w_{I21}	0.3	0.06
G_{22}	w_{I22}	0.2	0.05
G_{23}	w_{I23}	0.75	0.035
G_{31}	w_{I31}	0.07	0.09
G_{32}	w_{I32}	0.05	0.1

Table 11: The uncertainty model of the first order plus dead time components of $G(s)$

Figure 21 and Figure 22 graphically illustrates the procedure of fitting the uncertainty curves. The complete set of fitted figures can be found in the Appendix.

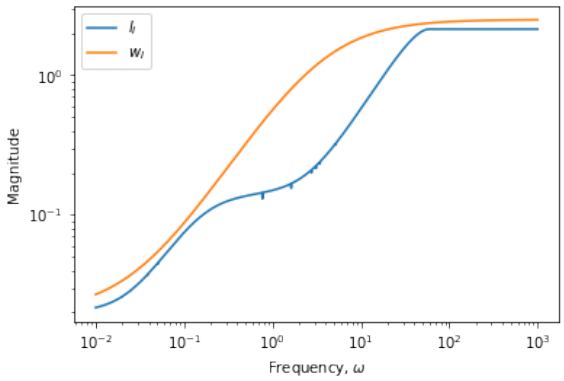

Figure 21: The uncertainty weight of transfer function G_{11}.

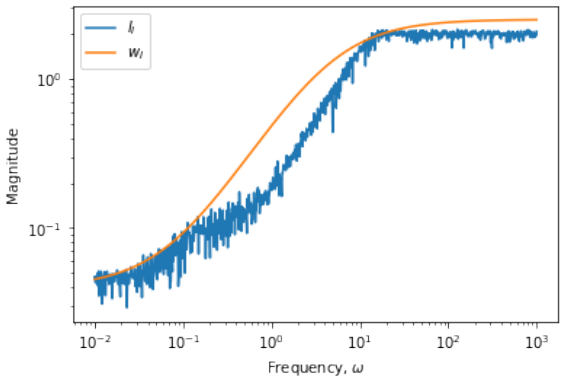

Figure 22: The uncertainty weight of transfer function G_{13}.

From Figure 22 it is apparent that the optimization function used to solve the "worst case" combination of the parameters did not return a smooth solution. Increasing the

number of start for the optimization function had no effect. In fact, al the functions with negative gain did not return a smooth curve when passed to the optimization function. Unfortunately, due to time constraints, the matter could not be investigated any further. The performance weight was just adjusted to lie on the top part of the fluctuating curve.

The transfer function G_{33}, required special attention, as this was not simply a first order plus dead time model. There are more time constants (a total number of three) in the function. All variables carried the same uncertainty as specified above. The ultimate performance weight function was determined as

$$w_{I33} = \frac{(0.8s + 8)(0.55s + 0.0095)}{(11s + 1)(0.015s + 1)} \tag{42}$$

The fitting of the uncertainty weight to l_I is displayed in Figure 23.

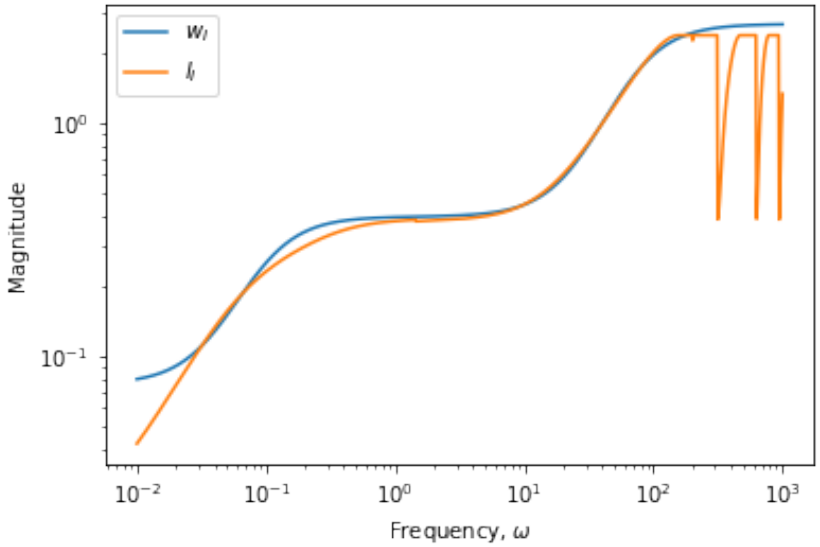

Figure 23: The uncertainty weight of transfer function G_{33}.

A much tighter uncertainty weight fit was achieved using this model. The weight described in Equation 41 was too inaccurate. Big over estimates would have been made at very low frequencies, as well as at crossover frequencies.

The same procedure was carried out to construct an uncertainty model for $G_d(s)$. There were again a lot of first order plus dead time elements in the system. Equation 41 was used to fit all of the multiplicative uncertainty descriptions. Table contains the resulting calculated constants.

Transfer Function	Uncertainty Weight	T	k_1
G_{d11}	w_{Id11}	1.5	0.01
G_{d21}	w_{Id21}	0.8	0.015
G_{d31}	w_{Id31}	0.8	0.015
G_{d32}	w_{Id32}	0.8	0.015

Table 12: The uncertainty model of the first order plus dead time components of $G_d(s)$

In $G_d(s)$ there are also two transfer function equation that are more complicated. The multiplicative uncertainty form has a shape that will require two lags and two leads in an uncertainty weight. The additive uncertainty form however only requires two lags and one lead. The uncertainty form slected for these two elements was therefore the additive form. The uncertainty weights calculated are

$$w_{A12} = \frac{6.94(-0.3s + 1)}{(s + 1)^2} \tag{43}$$

and

$$w_{A22} = \frac{11(35s + 1)}{(9.65s + 1)^2} \tag{44}$$

Figure 24 and Figure 25 displays the uncertainty weights fit for the above two equations.

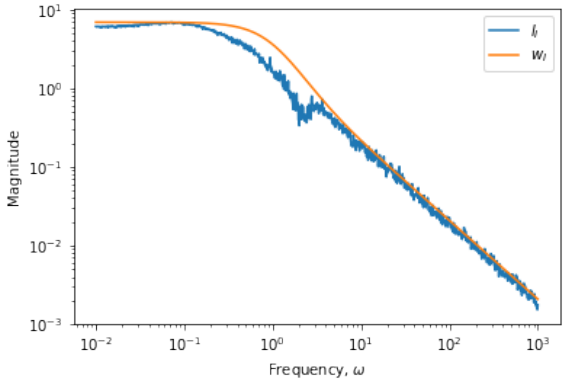

Figure 24: The uncertainty weight of transfer function Gd_{12}.

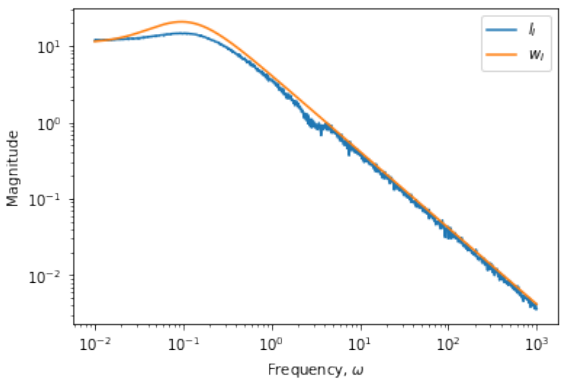

Figure 25: The uncertainty weight of transfer function Gd_{22}.

6 Performance Measurement

In order to adequately test the performance the system (nominal and robust performance), and acceptable and relative performance weight has to be formulated. This section entails the development of just such a function.

One major consideration in the performance weights are the disturbance dynamics. When designing a controller that has to reject disturbances up to an acceptable degree, the performance weight (w_P)can be chosen to closely represent G_d in SISO systems. Dosing this for MIMO is slightly harder, as the directions of the various disturbances play a major role in the disturbance rejection dynamics. Simply taking the singular value of G_d does not represent the disturbance inputs adequately.

Rejecting the disturbances, however, is not the only consideration. The performance of set-point tracking dynamics also has to be taken into account. A major role player in analysing this is the bandwidth limits calculated for all of the different inputs (see Section 3.7). A common choice for the form of the performance weight is

$$W_P = \text{diag}\{w_{Pi}\} \tag{45}$$

where

$$w_{Pi} = \frac{s/M_i + \omega^*_{Bi}}{s + \omega^*_{Bi} A_i}, A_i < 1 \tag{46}$$

Using Equation 46, and selecting a small value for A_i ensures approximate integral action when analysing the weighted sensitivity at very low frequencies ($\omega = 0$). M_i is mostly selected as 2. This value limits the required performance at high frequencies, and at the crossover frequencies, where $\sigma(S(j\omega)) > 1$. For this preliminary performance weight analysis, the value for M_i was chosen to be a constant 2. The bandwidths were chosen as the bandwidth limits outlined in Section 3.7. The value of A_i was chosen so that $A_i - \sigma_i(S(j10^{-2})) = 0$. Using this equation will ensure very tight performance requirements between the frequencies $\omega = 10^{-2}$ and ω^*_{Bi}, for all of the output variables.

The proposed performance weight equation is

$$W_P = \begin{bmatrix} \frac{s/2+0.46}{s+0.46(0.079)} & 0 & 0 \\ 0 & \frac{s/2+0.46}{s+0.46(0.395)} & 0 \\ 0 & 0 & \frac{s/2+1}{s+1(0.692)} \end{bmatrix} \tag{47}$$

7 Conclusions

Following the controllability analysis performed it can be stated that

1. The process contains good controllability characteristics. The bandwidth limitations on the process are reasonable, and will allow for the implementation of a controller.
2. The bounds set on disturbance variation were too ambitious, and the process may not be able to reject disturbances with magnitude close to the upper or lower bounds.
3. The bounds set on maximum set-point variation also appeared to be too ambitious. Especially the maximum set-point variation of 8 °C on the bottom tray temperature will not be realizable in the system.
4. The unstable nodes in the MIMO system were calculated and analysed successfully.
5. An acceptable uncertainty model was constructed to describe the various uncertainties within the model.
6. A performance weight was constructed to measure the nominal and robust performance of the process once the controller design has begun.

Recommendations and processes that will have to follow are

1. The controller for the process will have to be designed, using various methods (decentralized, H^{∞}-design).
2. When a controller transfer function has been designed, the nominal and robust stability and performance of the process has to be verified.
3. After the analysis and design, the implementation of the controller can commence.

References

Green, GW and Perry, RH (2007) *Perry's Chemical Engineer's Handbook*, 8th ed. MacGraw-Hill, New York.

Henstra, AM, Sipma, J, Rinzema, A and Stams, AJM (2007) "Microbiology of synthesis gas fermentation for biofuel production" *Elsevier*, *18 (3)*, 200 *206*.

Ogunnaike, BA, Lemaire, JL, Morari, M and Ray, WH (1983) "Advanced Multivariable Control of a Pilot Plant Distillation Column" *AIChE Journal*, *29 (4)*, 632 *639*.

Skogestad, S and Postlethwaite, I (2001) *Multivariable Feedback Control: Analysis and Design*, 2nd ed. John Wiley & Sons, New York.

Wankat, PC (2012) *Separation Process Engineering*, 3rd ed. Prentice Hall, New Jersey.

A Appendix

The figures below contain all the fitting curves used to obtain the uncertainty weights.

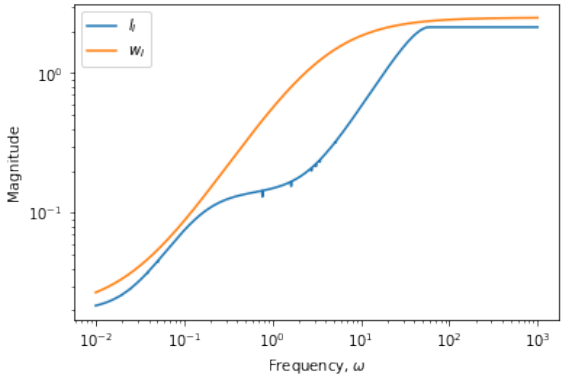

Figure 26: The uncertainty weight of transfer function G_{11}.

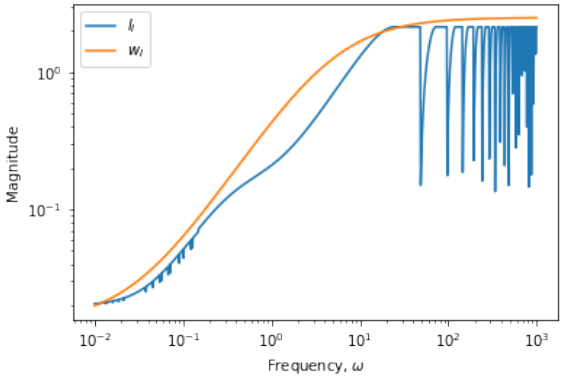

Figure 27: The uncertainty weight of transfer function G_{12}.

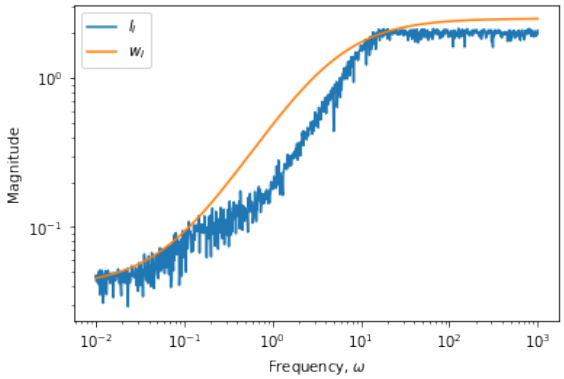

Figure 28: The uncertainty weight of transfer function G_{13}.

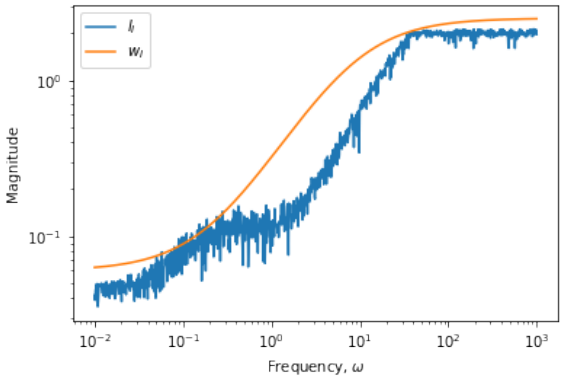

Figure 29: The uncertainty weight of transfer function G_{21}.

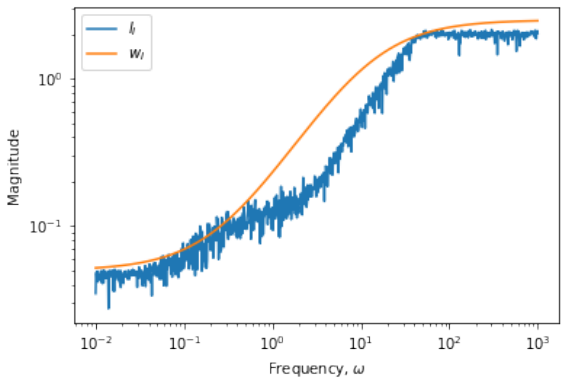

Figure 30: The uncertainty weight of transfer function G_{22}.

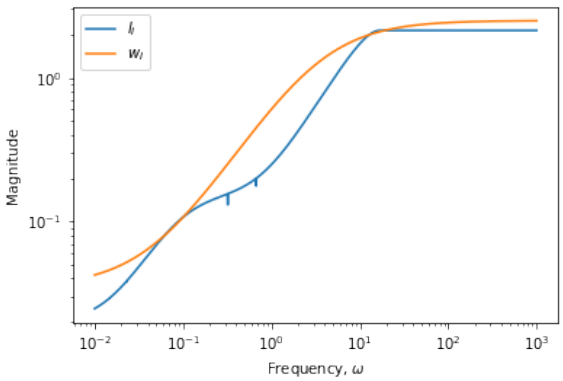

Figure 31: The uncertainty weight of transfer function G_{23}.

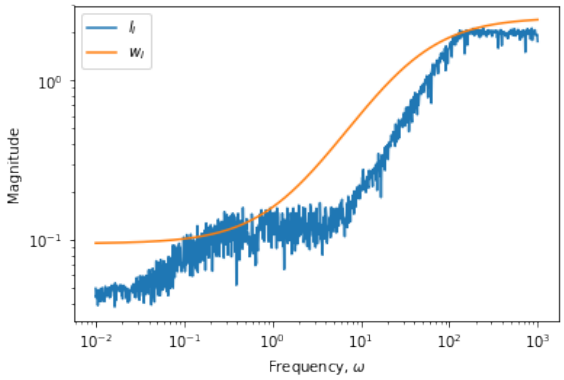

Figure 32: The uncertainty weight of transfer function G_{31}.

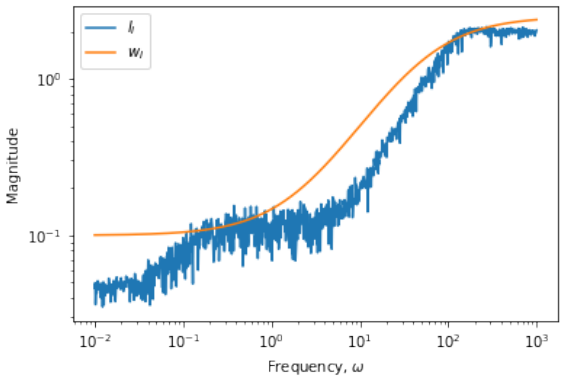

Figure 33: The uncertainty weight of transfer function G_{32}.

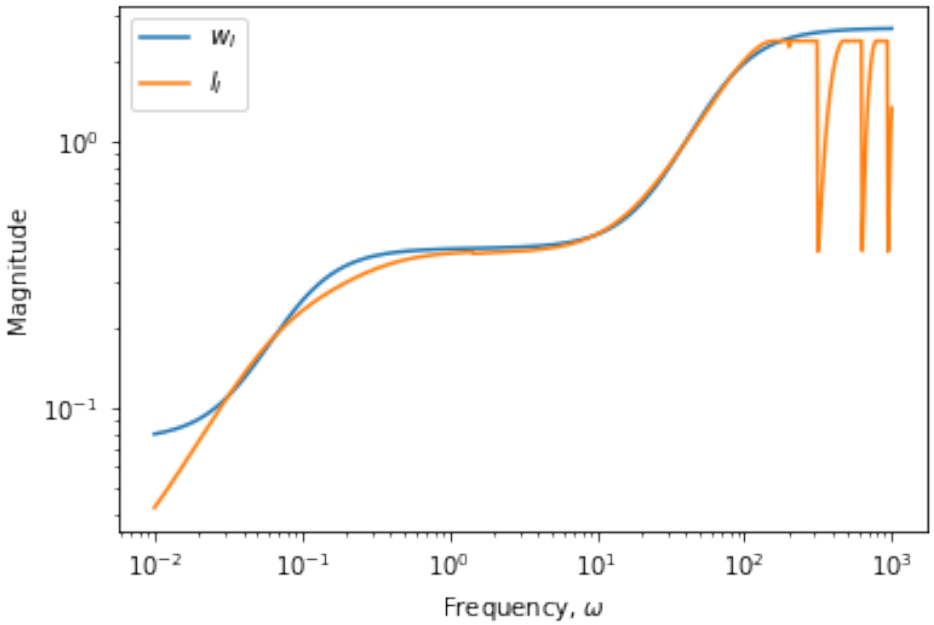

Figure 34: The uncertainty weight of transfer function G_{33}.